EARTHQUAKE ENGINEERING AND STRUCTURAL DYNAMICS, VOL. 26, 423–439 (1997)

DAMAGE MODELS FOR THE SEISMIC RESPONSE OF BRICK MASONRY SHEAR WALLS. PART I: THE MORTAR JOINT MODEL AND ITS APPLICATIONS

L. GAMBAROTTA AND S. LAGOMARSINO

Department of Structural and Geotechnical Engineering, University of Genoa, via Montallegro 1, 16145 Genoa, Italy

SUMMARY

The response of brick masonry walls to in-plane horizontal cyclic loads analogous to those induced during seismic events is analysed by applying constitutive models which take into account the mechanical behaviour of each component and its interfaces, i.e. decohesion and slipping in the mortar joints and failure in bricks. To this end, a damage model for mortar joints is proposed and then applied in two different approaches to the analysis of brick masonry walls which are described both in the present paper and in the companion paper.[1] The response of the mortar joint model to varying stress and strain is here analysed and applied to the simulation of experimental results from shear tests on mortar–brick assemblages. From the description of the mortar joints and assuming brittle constitutive equations for the brick units, a composite model based on a finite element approach is here developed and applied to the lateral analysis of rectangular shear walls. Even if this model turns out to be computationally burdensome, it may give information on the inelastic mechanisms and related strains by means of a local description of the element motion. Some simulations of the lateral response of experimented walls under cyclic horizontal actions superimposed on vertical loads are carried out and an interpretation of the influence of the wall geometry on the lateral stiffness degradation and on the hysteretic energy dissipation is given. © 1997 by John Wiley & Sons, Ltd.

KEY WORDS: masonry walls; constitutive equations; damage; brick–mortar interface; discrete models; hysteretic response

1. INTRODUCTION

It is well known that the seismic vulnerability of masonry buildings is strongly affected by the performance of the shear walls. When their out of plane failure is prevented by suitable devices, the prediction of the structural reliability and the selection of strengthening techniques may be carried out on the basis of the knowledge of the shear wall in-plane behaviour. This procedure justifies the interest of the researchers in modelling and experimenting the response of shear walls under horizontal cyclic actions, which is usually characterized by a peak load and stiffness degradation with marked hysteretic dissipation.[2]

Simple models that consider each wall as a single structural element characterized by a non-linear response in terms of applied shear and lateral drift[3,4] have been proposed. However, information about the influence of the wall shape and the compressive stress on the wall behaviour can only be obtained by referring to two-dimensional models and to proper constitutive equations for the brick masonry. In this context, some results concerning the lateral strength may be obtained by the continuum model for a medium with no tensile strength[5] or by the smeared crack approach[6]. Nevertheless, more detailed constitutive models must be considered to describe the strength of horizontal forces, the post-peak phase and the hysteretic response of walls; in fact, these features are strongly affected by the masonry pattern and by the mechanical characteristics of the components of the masonry, which is a composite material. This requires the preliminary development of constitutive models for each component, which may be detailed more or less according to the degree of accuracy of the proposed masonry model,[7] and for the brick–mortar interface where decohesion and frictional slipping take place. To this end three different approaches can be considered in order to obtain models available for different levels of complexity: simple masonry assemblages, simple panels and large-scale shear walls.

CCC 0098–8847/97/040423–17$17·50

Received 5 March 1996
Revised 11 October 1996

Apparently, the more direct approach considers brick units and mortar joints as continuum elements. In this case very refined finite element modelling together with constitutive equations able to take into account the brittle behaviour of the materials is required;[8] such models should be improved in order to describe the brick–mortar interface according to fracture mechanics theory. However, they are extremely burdensome from a computational point of view and the calibration of the model parameters from experimental data may not be well defined.

An interesting approach considers the mortar joints, the weakest components of the brickwork, by means of an interface: a discontinuity element connecting the brick units.[9–12] This assumption implies that the damage and failure of brick units need to be properly modelled. In fact, the brick model must also include the compressive failure of the masonry, which actually involves both bricks and mortar, because the interface model ignores the Poisson effect and thus only partially describes the brick–mortar interaction. On these bases, the masonry may be analysed by a 'composite' scheme, that allows the wall response to horizontal actions superimposed on vertical forces to be simulated accurately through finite element models. Also, this approach turns out to be computationally intensive because of the description of each brick by means of several finite elements; thus, its application is limited to small panels.

On the other hand, the analysis of large-scale shear walls requires a simpler approach, generally based on a continuum description, which considers the two-phase brick masonry represented by the constitutive equations of an equivalent homogeneous medium whose characteristics have to be obtained through homogenisation procedure. To this end different continuum models have been proposed,[13–18] some of them only concerning the elastic characterization of the brick masonry.[16,17] Nevertheless, those models have not been applied to the analysis of shear walls and most of them do not take into account the influence of the compressive stress on the masonry response.

The modelling of in-plane loaded brick masonry shear walls is considered in the present paper through a composite model, while in the companion paper[1] a continuum damage model is proposed and applied to the analysis of large-scale walls. Both the approaches are based on a mortar joint interface model which is presented in Section 2 of the present paper. This model is based on damage mechanics and takes into account both the mortar damage and the brick–mortar decohesion, which are considered to take place when opening and frictional sliding are activated. The constitutive equation of the interface is postulated in terms of two internal variables representing the frictional sliding and the mortar joint damage. The evolution of such variables is ruled both by a friction limit and by a damage condition. In particular, to allow the application of the model in finite element procedures, an integration algorithm of the constitutive equation in the finite load step has been formulated. The obtained mortar joint model, which exhibits a brittle response under tensile stresses, is characterized by frictional dissipation together with stiffness degrading under compressive stresses, as shown by some examples and simulations of experimental tests on brick mortar assemblages. Moreover, by a comparison with the typical experimental results from the triplet tests, the model parameters can be easily identified. These aspects encourage the adoption of the interface model as a tool for interpreting the fundamental aspects of the stiffness degrading and hysteretic dissipation exhibited by brick masonry walls.

The mortar joint model is the base of a composite finite element model in which brick units and mortar joints are described separately (Section 3). The former are modelled by isoparametric elements connected by interfaces located in both bed and head mortar joints. In particular, the brick units are modelled as elastic–plastic solids having brittle interfaces located to correspond with the head joints of the neighbouring layers.

Some simulations of experimental tests on rectangular panels[2] have been carried out (Section 4) showing the reliability of the method. In fact the composite model can simulate the most significant aspects of the response of masonry panels and may be used to validate the continuum model presented in the companion paper.[1]

2. A DAMAGE MODEL FOR MORTAR JOINTS

Referring to the brick masonry shown in Figure 1, let us consider a mortar joint having thickness s, included between bricks. This assemblage corresponds to the samples usually tested by Atkinson *et al.*,[19] van der Pluijm[20] and Binda *et al.*[21] in order to characterize the response of mortar joints.

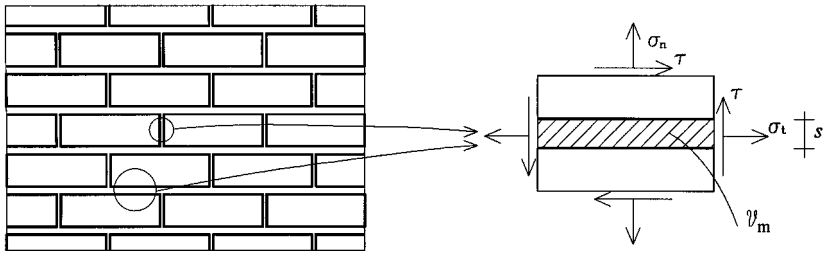

Figure 1. Brick masonry, mortar joint and stress components

In order to describe both the mortar damage and the decohesion in the mortar–brick interface as a whole, mean strain and stress are considered in the representative volume element $\mathscr{V}_m$ including the mortar and the brick–mortar interface.[22] The mean strain $\boldsymbol{\varepsilon}_m = \{\varepsilon_t, \varepsilon_n, \gamma\}^t$, assumed to depend on the mean stress $\boldsymbol{\sigma}_m = \{\sigma_t, \sigma_n, \tau\}^t$ (σ_n and τ being the components of the resolved stress on the joint plane), may be split into the elastic and inelastic components:

$$\boldsymbol{\varepsilon}_m = \mathbf{K}_m \boldsymbol{\sigma}_m + \boldsymbol{\varepsilon}_m^* \tag{1}$$

where $\mathbf{K}_m$ is the elastic compliance matrix of the mortar (depending on its elastic moduli E_m and ν_m) and $\boldsymbol{\varepsilon}_m^* = \{0, \varepsilon_m^*, \gamma_m^*\}^t$ collects the inelastic extension and sliding of the mortar joint. Denoting the joint damage variable as α_m ($\geqslant 0$), these strain components are assumed as follows:

$$\varepsilon_m^* = h(\alpha_m)\, H(\sigma_n)\, \sigma_n \tag{2a}$$

$$\gamma_m^* = k(\alpha_m)\, (\tau - f) \tag{2b}$$

where $h(\alpha_m)$ and $k(\alpha_m)$ are positive functions representing the opening and sliding compliances of the mortar joint, which increase with the damage variable from the initial undamaged state $h(0) = k(0) = 0$. In equation (2a), the Heaviside function $H(\sigma_n)$ takes into account the unilateral response of the joint. Finally, the variable f is representative of the friction in the mortar–brick interface,[23] that is the internal force in the compressed joint ($\sigma_n < 0$) limiting or locking the sliding, and the remaining part of the internal force $(\tau - f)$ is here considered as inducing damage in the elastic matrix. The constitutive assumptions expressed by equations (1) and (2) ignore both the effects of the stress σ_t on the inelastic strain components and the mechanisms activating the corresponding strain ε_t^*.

Equations (1) and (2) imply that the internal variables α_m and f must be known at any step of the loading history through evolution equations. To this end, it is worth noting that, according to Reference 23, the variables γ_m^* and α_m are associated with f and Y_m, respectively, the latter being the energy release rate of mortar joint damage defined as follows:

$$Y_m = \tfrac{1}{2} h'(\alpha_m) H(\sigma_n)\, \sigma_n^2 + \tfrac{1}{2} k'(\alpha_m)(\tau - f)^2 \tag{3}$$

where $h' = \mathrm{d}h/\mathrm{d}\alpha$ and $k' = \mathrm{d}k/\mathrm{d}\alpha$. The evolution equations of the internal variables are formulated on the basis of two conditions to be satisfied at any time in the loading process.

The variable f has to satisfy the friction limit condition

$$\phi_s = |f| + \mu\sigma_n \leqslant 0 \tag{4}$$

involving the friction coefficient μ, with which the simple flow rule

$$\dot{\gamma}_m^* = v\dot{\lambda}, \quad \dot{\lambda} \geqslant 0 \tag{5}$$

is associated ($v = f/|f| = \pm 1$). The hypothesis of ignoring the extension induced by the frictional sliding, i.e. the joint dilation, is postulated because of the wide dependence of this phenomenon on the entity of the compressive stress σ_n and the deformation process. In fact, experimental results[20,21] showed that, by

increasing the compressive stress and the total inelastic strain, a transition from the joint dilation to joint compaction takes place, which would require a complex formulation to express the dependence of the ratio $\dot{\varepsilon}^*_m/\dot{\gamma}^*_m$, on the compressive stress[24,25] and on the strain history.

The damage evolution is defined, in accordance to the R-curve approach, which is used in the theory of fracture mechanics by imposing the damage energy release rate to be less than or equal to the mortar joint toughness R_m (assumed as depending on α_m), i.e.

$$\phi_{dm} = Y_m - R_m \leqslant 0 \tag{6}$$

When the limit condition is attained ($\phi_{dm} = \dot{\phi}_{dm} = 0$) the joint damage rate ($\dot{\alpha} \geqslant 0$) is assumed to take place in the infinitesimal load step. This is based on the assumption that damage can increase only when the available energy release rate Y_m equals the energy rate R_m that would be dissipated during a damage process.

Due to the complexities of the damaging mechanisms in the mortar joint, the compliance functions $h(\alpha_m)$ and $k(\alpha_m)$ cannot be deduced on a mechanical basis. Consequently, the following simple assumption, implying Y_m to be independent of α_m, is accepted:

$$h(\alpha_m) = c_{mn}\,\alpha_m, \quad k(\alpha_m) = c_{mt}\alpha_m \tag{7}$$

When a tensile stress is active on the mortar joint ($\sigma_n \geqslant 0$), condition (6) may be rewritten as follows:

$$\phi^+_{dm} = \tfrac{1}{2}c_{mn}(\sigma_n^2 + \rho_m\tau^2) - R_m(\alpha_m) \leqslant 0 \tag{8}$$

where $\rho_m = c_{mt}/c_{mn}$. Once the stress state and the function $R_m(\alpha_m)$ are given, the damage variable α_m can be evaluated by solving equation $\phi^+_{dm} = 0$.

As may be argued from the diagrams in Figure 2, representing Y_m and R_m in terms of α_m, the existence of a limit state representative of the mortar joint failure is subordinate to the existence of a maximum R_{mc} of the toughness function $R_m(\alpha_m)$ (point B); given the arbitrariness of the intensity of the damage variable, to characterize this state the reference value $\alpha_{mc} = 1$ is assumed here. Considering the irreversibility of the damage process ($\dot{\alpha}_m \geqslant 1$), the phase preceding the limit state B ($R'_m = dR_m/d\alpha > 0$) exhibits a unique stable response (see for instance point A). On the other hand, the subsequent phase ($R'_m < 0$) under stress control provides two solutions (see point C). In fact, by diminishing Y_m from point C, due to a lowering of the stress level, condition, (6) and (8) are fulfilled both by damage arrest and by damage evolution, as these two solutions correspond to different strain rates. To guarantee the irreversibility of the inelastic strain rate $\dot{\varepsilon}^*_m \geqslant 0$, the function R_m must satisfy the following condition:

$$2R_m(\alpha_m) + \alpha_m R'_m(\alpha_m) > 0, \quad \forall\alpha_m > 0 \tag{9}$$

and in the post-peak phase it must vanish for α_m increasing. It follows that the failure condition of the mortar joint under tensile stresses is obtained as the limit state $\phi^+_{dm}(\alpha_m = 1) = 0$ which

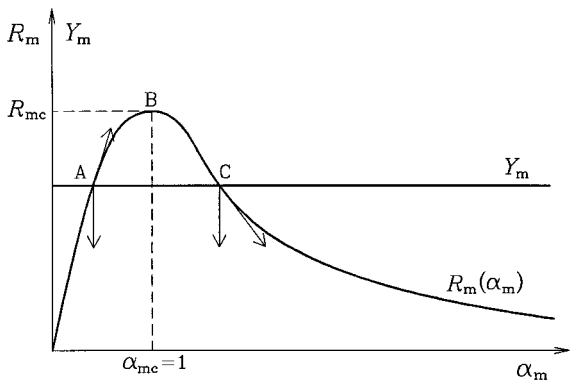

Figure 2. Damage function for the mortar joint; stable and unstable evolution

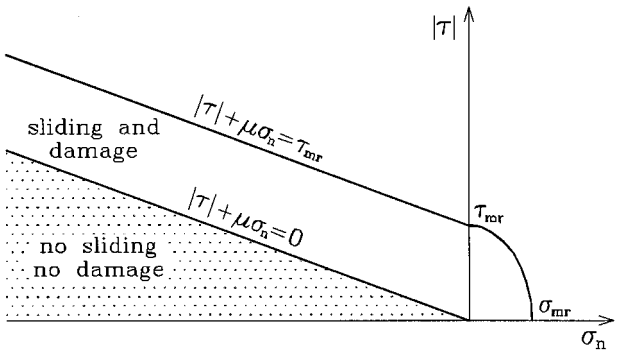

Figure 3. Limit strength domain and elastic domain in the $(\sigma_n, |\tau|)$ plane

corresponds to:

$$\sigma_n^2 + \rho_m \tau^2 = 2R_{mc}/c_{mn} = \sigma_{mr}^2 = \rho_m \tau_{mr}^2 \tag{10}$$

where σ_{mr} and τ_{mr} represent the tensile and shearing strength of the mortar joints.

If the compressive stress acts on the joint ($\sigma_n < 0$), then the sliding $\dot{\gamma}_m^*$ and damage $\dot{\alpha}_m$ rates must be evaluated considering conditions (4) and (6) which, through assumptions (2) and (7), become

$$\phi_s = |\tau - \gamma_m^*/c_{mt}\alpha_m| + \mu\sigma_n \leqslant 0 \tag{11}$$

$$\phi_{dm}^- = \tfrac{1}{2}\gamma_m^{*2}/c_{mt}\alpha_m^2 - R_m(\alpha_m) \leqslant 0 \tag{12}$$

If the friction limit condition $\phi_s = 0$ is reached, two different evolutions are possible in the infinitesimal load step. If $\phi_{dm}^- < 0$, only sliding $\dot{\gamma}_m^*$ can take place and its entity may be evaluated as the solution of a linear complementary problem. This happens when the total sliding is lesser than the maximum attained during the damage process, which is responsible for the present damage. Otherwise, if $\phi_{dm}^- = \dot{\phi}_{dm}^- = 0$, sliding $\dot{\gamma}_m^*$ and damage $\dot{\alpha}_m$ rates may occur; also in this case the solutions in the infinitesimal load step are obtained from a linear complementary problem, whose solution may be single or double according to $R'_m > 0$ or $R'_m < 0$, respectively. On the other hand it is worth noting that damage evolution without sliding is not possible because condition (12) depends only on the internal variables and not on the applied stress.

Since before sliding the applied shearing stress τ is completely sustained by the internal friction f, it follows from equation (4) that the no-sliding condition is

$$|\tau| + \mu\sigma_n \leqslant 0 \tag{13}$$

Once this limit condition is attained, sliding and damage take place. The failure condition is obtained with reference to proportional loading histories in which $f = -\mu\sigma_n\tau/|\tau|$; this term substituted in equations (2b), (7) and finally in $\phi_{dm}^-(\alpha_m = 1) = 0$ allows the obtaining of the failure limit condition:

$$|\tau| + \mu\sigma_n \leqslant \tau_{mr} \tag{14}$$

Once the model parameters σ_{mr}, τ_{mr} and μ are assigned, both the limiting resistance domains, delimited by the conditions (10) and (14), and the limiting sliding domain, expressed by the condition (13), are defined in the plane $(\sigma_n, |\tau|)$, as shown by Figure 3.

2.1. Integration of the constitutive model in the finite load step

The application of the previously described damage model in the finite element analysis of shear masonry walls under arbitrary loading paths and particularly under cyclic load histories requires the formulation of a procedure for the integration of the constitutive equations in the finite load step.[26]

Considering a reference state characterized by given values of the state variables ($\boldsymbol{\varepsilon}$, $\boldsymbol{\sigma}$, ε_m^*, γ_m^*, α_m) and assuming the strain increment $\Delta\boldsymbol{\varepsilon}$ as given, the problem concerns the determination of the corresponding

increments of the state variables ($\Delta\boldsymbol{\sigma}$, $\Delta\varepsilon_m^*$, $\Delta\gamma_m^*$, $\Delta\alpha_m$). Since the constitutive equations are markedly different if compressive or tensile stress is acting on the joint plane, these two events are distinguished in the finite step by observing by equations (1), (2) and (7) that $\mathrm{sgn}(\sigma_n) = \mathrm{sgn}(v_m\varepsilon_t + \varepsilon_n)$. Thus, on the assumption of a proportional increment of the imposed strain components, it is possible to select substeps each one referred to tensile or compressive stress on the joint plane.

The case of tensile stress ($\sigma_n \geqslant 0$) is tackled by assuming the load step with no damage evolution ($\Delta\alpha_m = 0$) and so obtaining the trial stress state:

$$\boldsymbol{\sigma}_t = (\mathbf{K}_m + \alpha_m\mathbf{K}_m^*)^{-1}\boldsymbol{\varepsilon}_f \tag{15}$$

where $\boldsymbol{\varepsilon}_f = \boldsymbol{\varepsilon} + \Delta\boldsymbol{\varepsilon}$ and $\mathbf{K}_m^*$ is the inelastic compliance matrix whose non-vanishing components are $K_{m22}^* = c_{mn}$ and $K_{m33}^* = c_{mt}$. Then, if the condition

$$\phi_{dm}^+(\boldsymbol{\varepsilon}_f, \alpha_m) = \tfrac{1}{2}\boldsymbol{\varepsilon}_f^t(\mathbf{K}_m + \alpha_m\mathbf{K}_m^*)^{-t}\mathbf{K}_m^*(\mathbf{K}_m + \alpha_m\mathbf{K}_m^*)^{-1}\boldsymbol{\varepsilon}_f - R_m(\alpha_m) \leqslant 0 \tag{16}$$

which is expressed in terms of the imposed strain $\boldsymbol{\varepsilon}_f$ at the end of the step and obtained by substituting equation (15) in equation (8), is satisfied, the trial stress turns out to be the final one $\boldsymbol{\sigma}_f = \boldsymbol{\sigma}_t$. On the other hand, if $\phi_{dm}^+(\boldsymbol{\varepsilon}_f, \alpha_m) > 0$ is obtained, a damage evolution ($\Delta\alpha_m > 0$) in the step must be considered and the final value $\alpha_m + \Delta\alpha_m$ of the damage variable has to be obtained by solving the non-linear equation $\phi_{dm}^+(\boldsymbol{\varepsilon}_f, \alpha_m + \Delta\alpha_m) = 0$. Once the damage variable is updated, the final stress state $\boldsymbol{\sigma}_f$ can be evaluated from equation (15).

Also the case of compressed joint ($\sigma_n < 0$) is carried out by considering a first trial phase in which both sliding ($\Delta\gamma_m^* = 0$) and damage evolution ($\Delta\alpha_m = 0$) are excluded; the stress increment turns out to be $\Delta\boldsymbol{\sigma} = \mathbf{K}_m^{-1}\Delta\boldsymbol{\varepsilon}_f$, first allowing the trial of the stress vector $\boldsymbol{\sigma}_t = \boldsymbol{\sigma} + \Delta\boldsymbol{\sigma}$ and then the final values of the normal stress components $\sigma_{nf} = \sigma_{nt}$ and $\sigma_{tf} = \sigma_{tt}$. If the trial stress $\boldsymbol{\sigma}_t$ satisfies both the conditions (11) and (12) with the initial values of the variables γ_m^* and α_m, then the elastic prevision turns out to be verified and the final stress state is $\boldsymbol{\sigma}_f = \boldsymbol{\sigma}_t$. Otherwise, it follows that sliding takes place during the step with possible damage evolution, so implying a correction ($\Delta\tau_c$, $\Delta\gamma_m^*$, $\Delta\alpha_m$) of the variables which must be carried out according to a stress–strain path characterized by constant total shearing strain $\Delta\gamma_m = \Delta\gamma_{me} + \Delta\gamma_m^* = 0$. To this end it must be pointed out, on the basis of equations (1) and (5) referred to finite increments and being $v = \mathrm{sgn}(\tau_t - \gamma_m^*/c_{mt}\alpha_m)$ constant, that $\Delta\tau_c = -G_m\Delta\gamma_m^* = -G_m v\Delta\lambda$. Thus the correction of the variables has to be obtained as the solution of the non-linear complementary problem:

$$\phi_s(\tau_t + \Delta\tau_c, \gamma_m^* + v\,\Delta\lambda, \alpha_m + \Delta\alpha_m, \sigma_n) \leqslant 0 \tag{17a}$$

$$\phi_{dm}^-(\gamma_m^* + v\,\Delta\lambda, \alpha_m + \Delta\alpha_m) \leqslant 0 \tag{17b}$$

$$\Delta\tau_c = -G_m v\,\Delta\lambda \tag{17c}$$

$$\Delta\lambda \geqslant 0, \quad \Delta\alpha_m \geqslant 0 \tag{17d}$$

$$\phi_s\,\Delta\lambda = 0, \quad \phi_{dm}^-\,\Delta\alpha_m = 0 \tag{17e}$$

Through an iterative algorithm based on the Newton–Raphson method, which is similar to that proposed by Simo *et al.*,[27] the unknowns $\Delta\tau_c$, $\Delta\gamma_m^* = v\Delta\lambda$ and $\Delta\alpha_m$ can be obtained and thus the finite load step is solved by updating

$$\tau_f = \tau_t + \Delta\tau_c, \quad \gamma_{mf}^* = \gamma_m^* + \Delta\gamma_m^*, \quad \alpha_{mf} = \alpha_m + \Delta\alpha_m \tag{18}$$

2.2. Simulations of shear bond tests

To explain the behaviour of the mortar joint model, both the responses to tensile stress and to shearing strains superimposed on normal compressive stress are considered. Moreover, some experiments

have been simulated. The results in this section have been obtained by considering the following toughness function:

$$R_m(\alpha_m) = \begin{cases} R_{mc}\alpha_m & 0 < \alpha_m < 1 \\ R_{mc}\alpha_m^{-\beta} & \alpha_m > 1 \end{cases} \tag{19}$$

that asymptotically tends to vanish for α_m increasing if $\beta > 0$ and satisfies the condition (9) if $\beta < 2$.

The response to normal tensile stresses is shown in the non-dimensional diagram in Figure 4 involving the ratio σ_n/σ_{mr} between the mean applied stress and the joint tensile strength and the ratio $\varepsilon_n/\varepsilon_{mr}$ between the normal strain and the strain at failure. This behaviour is characteristic of simple damage models. When monotonically increasing strains are imposed, a non-linear response with strain softening after reaching peak load is obtained, while the unloading phase exhibits a linear response with vanishing residual strain and stiffness degradation depending on the imposed maximum strain.

The model response to shearing strains superimposed on normal compressive stress is more complex. The non-dimensional diagram in Figure 5, in which $\tau_{jr} = \tau_{mr} - \mu\sigma_n$ is the shear stress at failure and $\gamma_{jr} = \tau_{jr}[1 + G_m c_{mt}(1 + \mu\sigma_n/\tau_{jr})]/G_m$ is the corresponding shearing strain, shows that during the loading phase the response is elastic, i.e. without frictional sliding, until $\tau = -\mu\sigma_n$. Once this stress level is reached

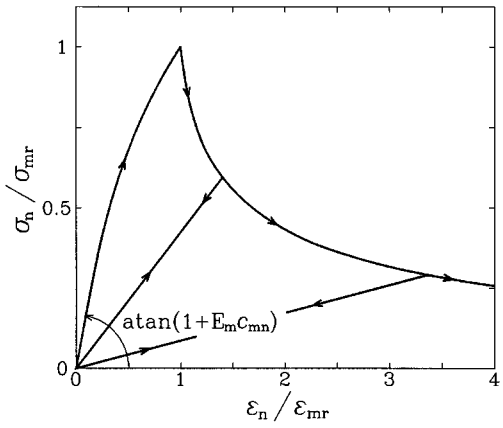

Figure 4. Response of the mortar joint model to tensile stresses

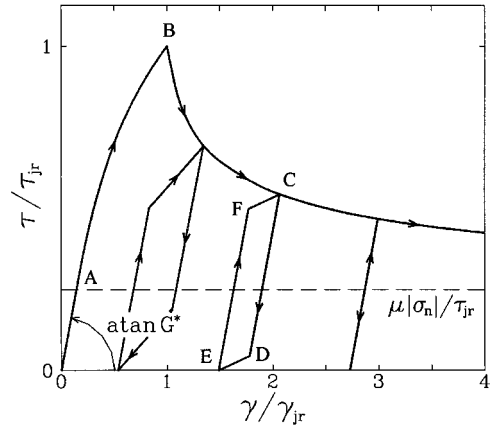

Figure 5. Model response to shearing strain superimposed on constant compressive stress

(point A), sliding and damage take place and the post-peak response (after the limit point B) is characterized by strain softening and the shear stress tends asymptotically to the limit value $\tau_1 = -\mu\sigma_n$. Moreover, the response to applied cyclic shearing strains turns out to be hysteretic according to a bilinear scheme. In fact, unloading is at first characterized by an elastic response, of stress amplitude $|\Delta\tau| = -2\mu\sigma_n$, with no sliding until the friction limit condition is reached (lines C–D, E–F), after which sliding takes place with reduced stiffness according to the damage level previously attained (lines D–E, F–C).

Finally, in the diagram of Figure 6 the typical response of the mortar joint model to applied cyclic shearing strain is shown and from this a bilinear response of the model emerges with the stiffness in the sliding phase ruled by the damage level.

The simulation of experimental results concerns shear tests carried out by Binda *et al.*[21] on triplets and by Atkinson *et al.* through a direct shear apparatus.[19]

In the former case the shear tests have been performed by assuming three bricks $55 \times 120 \times 170$ mm connected by two mortar joints 10 mm thick. After the preliminary compression in order to get a prescribed stress level, the central brick has been subjected to imposed lateral displacements. Some of the results from Reference 21 are shown in the diagrams of Figure 7(a) in terms of the mean shearing strain in the mortar joint and mean shear stress. Each diagram is referred to a prescribed normal stress σ_n (A: $-0{\cdot}12$ MPa, B: $-0{\cdot}4$ MPa, C: $-0{\cdot}8$ MPa, D: $-1{\cdot}25$ MPa) and further subjected to monotonically applied shearing strain. The good estimation of the shear stress at failure and of the post-peak behaviour emerges in Figure 7(b). The

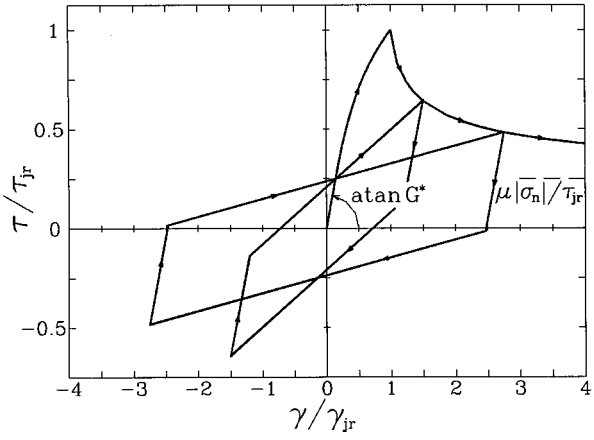

Figure 6. Model response to cyclic shearing strains

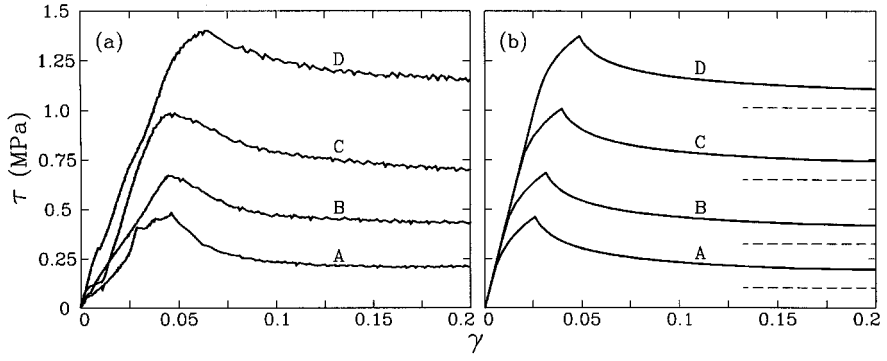

Figure 7. Tangential response of the brick-mortar joint: (a) experimental results from shear bond tests (triplets);[21] (b) theoretical simulation by the proposed model

irregular trend in the initial phase of the experiments may be due to the imperfect contact between the head of the brick and the jack.

The simulation by the theoretical model, shown in Figure 7(b), is obtained through the values of the parameters given in Table I. In Figure 8, the joint parameters τ_{mr} and μ are evaluated from the peak shear stresses, representative of the joint failure (Figure 7(a)), while the tangential elastic modulus G_m of the mortar is obtained by the initial response of the diagrams.

Finally, the proposed model has been applied to simulate the direct shear tests carried out by the experimental procedure proposed by Atkinson *et al.*,[19] which consists of a two layers assemblage of length equal to two bricks and is particularly effective in the characterization of the response to cyclic loading paths. Two different situations have been considered: (a) old bricks ($64 \times 100 \times 208$ mm) with a mortar joint 13 mm thick, subjected to the mean compressive stress on the joint $\sigma_n = -0{\cdot}33$ MPa; (b) new bricks ($55 \times 92 \times 193$ mm) with a bed joint thickness equal to 7 mm, subjected to the mean compressive stress on the joint $\sigma_n = -1{\cdot}34$ MPa; the characteristics of the constitutive elements (bricks and mortar) are summarized in Table II. The experimental results are represented in Figure 9 together with the theoretical ones, obtained by assuming the values of the model parameters given in Table III. The imposed shearing strains are very high in both cases if compared with the failure shearing strains; nevertheless the asymptotic shear stresses, due to friction, are not completely reached, due to a residual shear strength.

Table I. Model parameters assumed in the simulation of the experiments in Reference 21

G_m (MPa)	τ_{mr} (MPa)	μ	$1/c_{mt}$ (MPa)	β_m
40	0·36	0·81	25	0·7

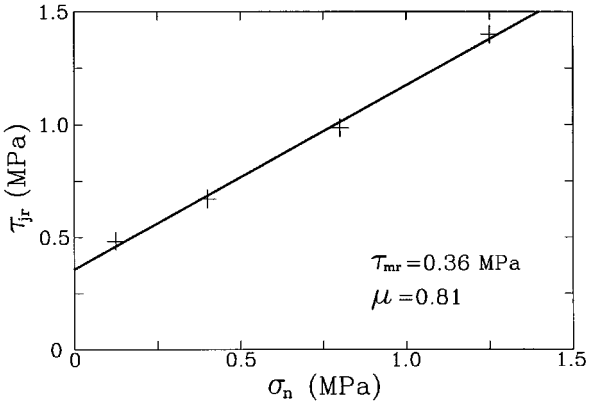

Figure 8. Failure limit domain of the experimented brick-mortar joint[21]

Table II. Dimensions and mechanical properties of the components[19]

	Brick (mm)	E_b (MPa)	ν_b	Joint (mm)	E_m (MPa)	ν_m
Old bricks	$208 \times 100 \times 64$	8796	0·16	13	1050	0·06
New bricks	$193 \times 92 \times 55$	14700	0·22	7	2110	0·05

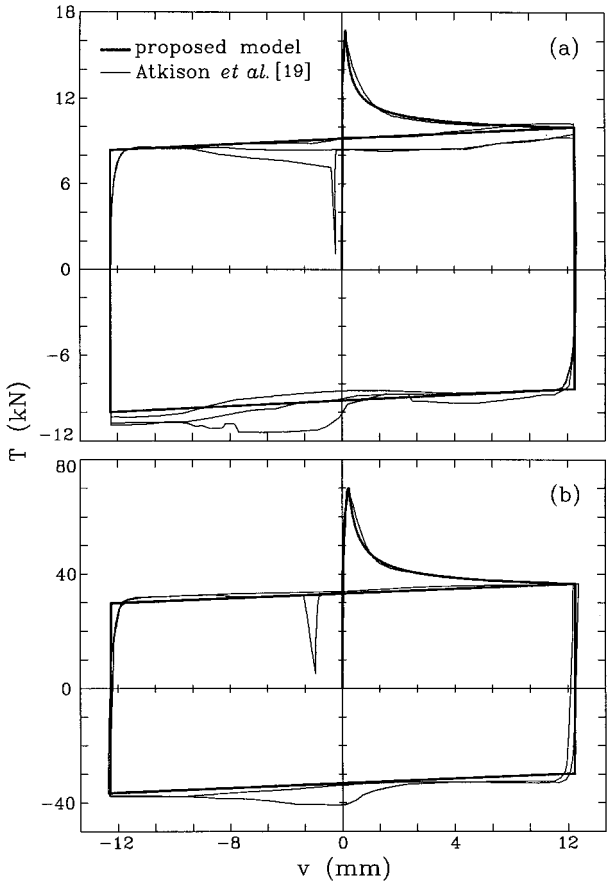

Figure 9. Simulations of the shear tests by Atkinson *et al.*:[19] (a) old bricks, (b) new bricks

Table III. Mortar joint model parameters

	G_m (MPa)	τ_{mr} (MPa)	μ	$1/c_{mt}$ (MPa)	β_m
Old bricks	495	0·18	0·67	12·5	0·8
New bricks	1005	1·0	0·67	20·0	0·8

3. COMPOSITE FINITE ELEMENT MODEL FOR BRICK MASONRY WALLS

Let us now consider the problem of modelling brick masonry walls under vertical constant loads applied to the top edge and successively by cyclic horizontal forces or displacements prescribed according to a defined history. These conditions are commonly prescribed in experiments[2–4,10,11] in order to evaluate the lateral strength of rectangular walls and are justified because they may be representative of the piers in masonry buildings. The experiments referred to in References 2–4 showed a lateral response characterized by stiffness degradation with increasing cycle amplitude, by the existence of a limit lateral strength, by strain softening and hysteretic response. Moreover, experiments on walls having different slenderness, i.e. height-to-width ratio, showed such effects to be more or less marked also as a consequence of the entity of the vertical forces. In particular, the response of squat walls seems to be more dissipative, while in slender walls the strain softening phase is less marked. These varieties of behaviour may be attributed to the activation of different

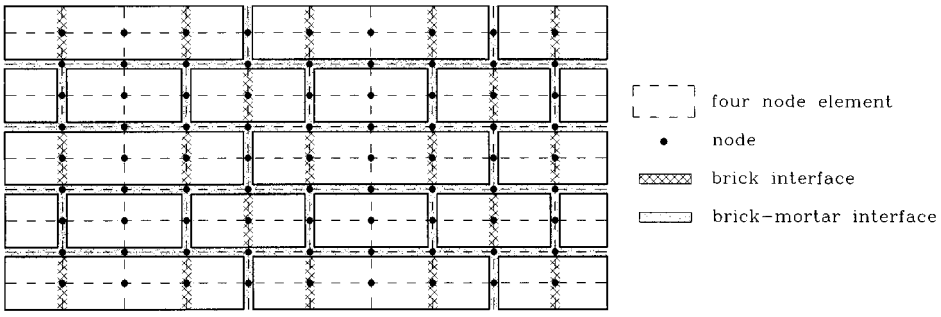

Figure 10. Finite element composite model of the masonry

mechanisms of inelasticity during the deformation process of the wall. Among these mechanisms, the more relevant ones are the opening and frictional sliding of mortar joints, the tensile and shearing rupture of bricks and the compressive failure of masonry.

In order to give a detailed description of such mechanisms, a composite model for the masonry wall has been developed, in which a two-phase system is considered made up of brick units and mortar joints. The former are modelled as rectangular domains connected by interfaces representative of the bed and head mortar joints. To this end a finite element model has been defined in which the brick units are modelled through four or eight isoparametric elements with four nodes while the mortar joints are modelled by interface element with four nodes, as shown in Figure 10.

The constitutive model assumed for the interface is the one described in Section 2 which gives both the joint opening under tensile stresses and the frictional sliding under compressive stresses on the joint. In particular, as a consequence of these constitutive equations and considering the vanishing thickness of the interface, the relative displacements in the interface can be expressed as follows:

$$\Delta \mathbf{u}_{\mathrm{m}} = \mathbf{D}_{\mathrm{m}} \boldsymbol{\sigma}_{\mathrm{m}} + \Delta \mathbf{u}^{*} \tag{20}$$

$\mathbf{D}_{\mathrm{m}}$ being the diagonal elastic compliance matrix of the interface (having modulus of normal compliance $d_{\mathrm{n}} = s/E_{\mathrm{m}}$ and shearing compliance $d_{\mathrm{s}} = s/G_{\mathrm{m}}$) and $\Delta \mathbf{u}^{*} = \{0, \Delta u_{\mathrm{n}}^{*}, \Delta u_{\mathrm{s}}^{*}\}^{\mathrm{t}}$ the vector of the inelastic normal and tangential relative displacements, which can be expressed according to the previously described model as follows:

$$\Delta u_{\mathrm{n}}^{*} = s c_{\mathrm{mn}} \alpha_{\mathrm{m}} H(\sigma_{\mathrm{n}}) \sigma_{\mathrm{n}} \tag{21a}$$

$$\Delta u_{\mathrm{s}}^{*} = s c_{\mathrm{mt}} \alpha_{\mathrm{m}} (\tau - f) \tag{21b}$$

In implementing the interface element, the two point Gauss integration scheme is applied since the relevant elastic compliance of the interface itself, compared to the corresponding one of the joint having equal width and made up of brick, does not require refined integration schemes.[28]

The constitutive model for the brick elements in the linear elastic phase is based on the isotropic assumption and the elastic moduli are selected in order to obtain a mean value of the normal and shearing strain equivalent to the corresponding one in the assemblage made up of one mortar joint and two half bricks. The post-elastic behaviour of bricks has been modelled by differentiating between the mechanism of tensile fracture of bricks and the mechanism of compressive failure of masonry. The former effect has been described by considering a potential vertical crack plane located to correspond with the head joint as shown in Figure 10. The crack plane is modelled by an interface analogous to that assumed for the mortar joints but ignoring, in this case, the friction effect ($f = 0$), and therefore obtaining a brittle description of the tensile and shearing fracture in the vertical crack plane. In this case the moduli of elastic compliance of the interface may be assumed by considering the same width of the head mortar joint, while the moduli of inelastic deformation can be obtained by tensile tests on bricks. The description of the compressive failure of masonry has been synthesised in the post-elastic model of the brick elements by considering that this process is characterized by

the tensile fracture of bricks as a consequence of the different transversal deformation both in the mortar joint and in the bricks. Since the interface model for the mortar joint is unable to describe such an effect, it has been taken into account as an overall effect in the constitutive equation of the bricks. To this end an elastic limit condition for the brick elements based on the von Mises criterion is assumed and the parameter selecting the limit state surface is obtained with reference to the failure under simple compression; moreover, a moderate strain softening is taken into account.

The interfaces representative of the potential cracks in the brick units are modelled through four-node elements having two Gauss points, while for the bricks, four-node isoparametric elements with a two Gauss point integration scheme are considered.

The model response to non-proportional load histories is carried out through an incremental-iterative finite element procedure[26] which allows both applied loads and prescribed displacements to be taken into account. In particular, an *initial stress* iterative procedure is applied in which a constant stiffness matrix corresponding to the undamaged wall is assumed; at any Gauss point of the interface the evolution of the stress and of the damage variable α_m and friction variable f is carried out through the procedure proposed in Section 2.1. Finally, in the Gauss point within the brick elements, the variables are up to date by applying the well-known radial return mapping procedure.

4. SIMULATIONS OF EXPERIMENTAL RESULTS

As an example, the results of tests carried out on two walls,[2] made up of the same constitutive elements and masonry pattern but characterized by different slenderness, have been considered and simulated by using the finite element model described in the previous section. Since in real cases rotations at the storey levels are

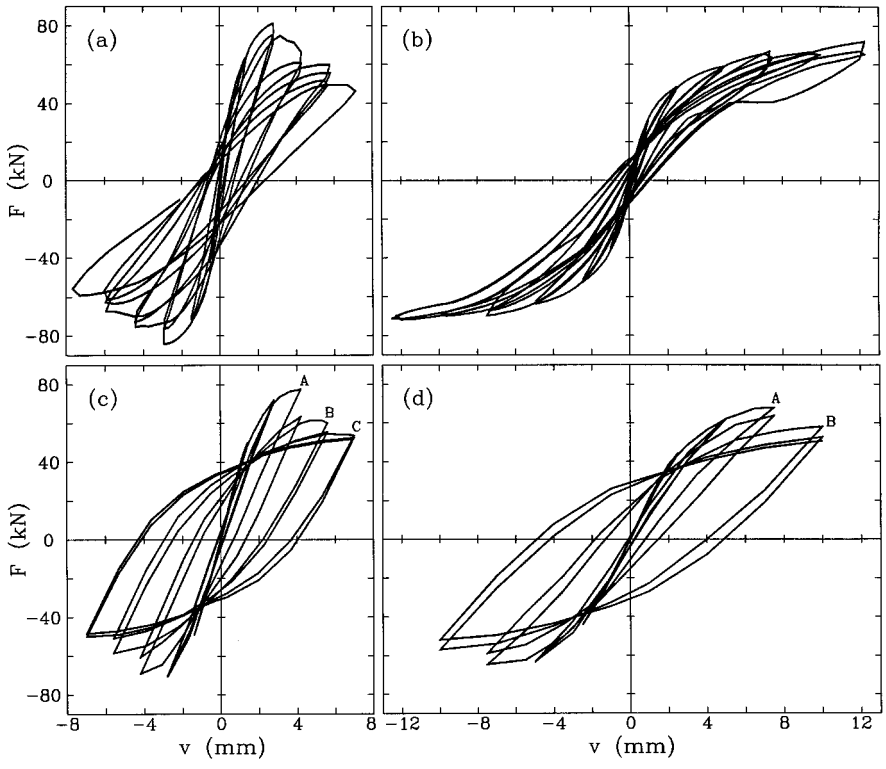

Figure 11. Rectangular masonry panels. Experimental response to horizontal actions:[2] (a) *low wall*; (b) *high wall*. Theoretical response by the composite model: (c) *low wall*; (d) *high wall*

usually moderate, the experimental set-up is such that rotation at the top edge is inhibited, so allowing vertical and horizontal displacements.

The masonry is made of $55 \times 120 \times 250$ mm bricks and the thickness of the mortar joints is $s = 10$ mm; the masonry pattern is the English bond and the thickness of the two walls is 25 cm. The first wall (*low wall*) is 100 cm wide and 135 cm high while the other is 200 cm high (*high wall*). Both the walls were initially compressed by a vertical load of 150 kN, corresponding to a medium vertical stress of 0·6 MPa. The experimental results are shown in Figures 11(a) and 11(b) in terms of the applied lateral deflection v to the top

Table IV. Model parameters assumed in the composite model

	E_m (MPa)	G_m (MPa)	σ_{mr} (MPa)	τ_{mr} (MPa)	μ	$1/c_{mt}$ (MPa)	β_m
Mortar joints	530	100	0·1	0·4	0·3	200	0·8
	E_b (MPa)	G_b (MPa)	σ_{br} (MPa)	τ_{br} (MPa)	μ_b	$1/c_{bt}$ (MPa)	β_b
Brick interface	2400	1000	0·4	1·2	0·0	100	0·8

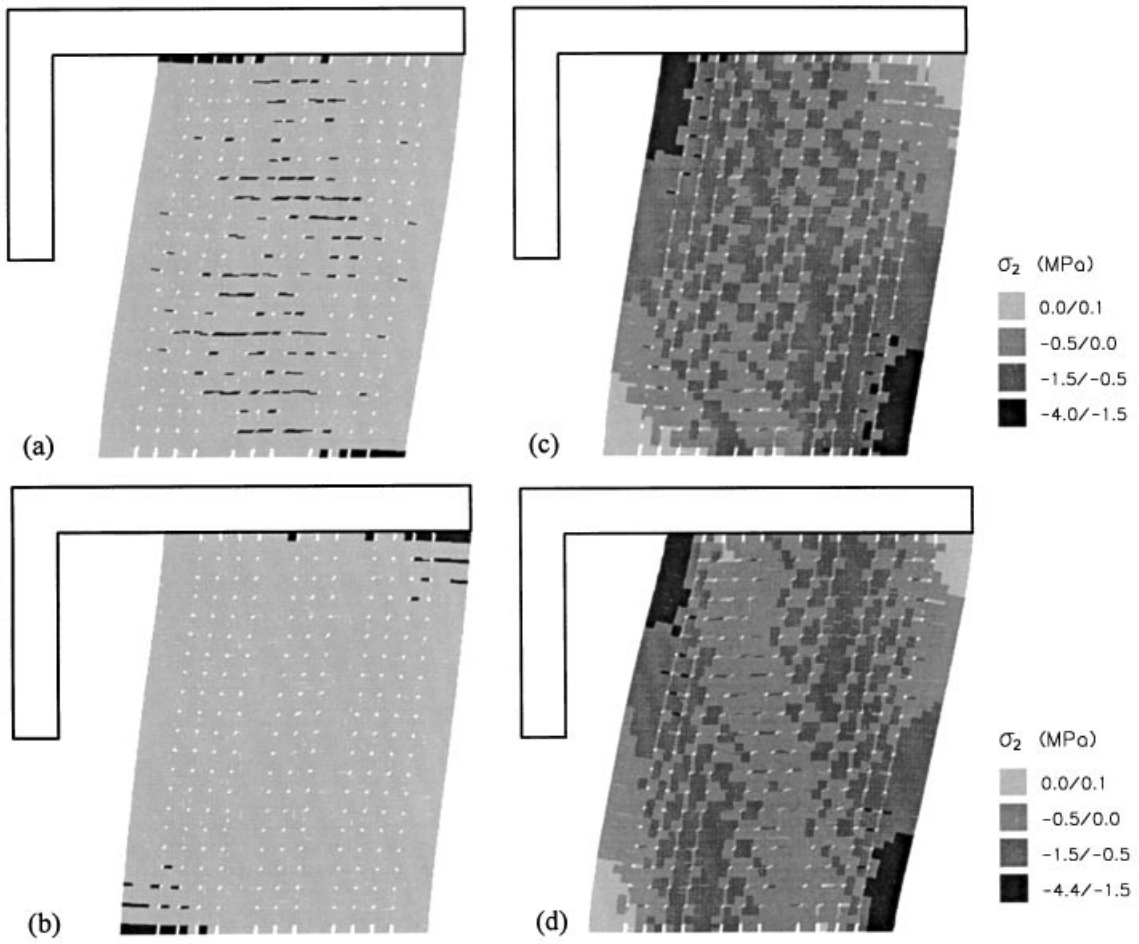

Figure 12. *Low wall*. State A: (a) sliding rupture of mortar joints; (b) opening rupture of mortar joints; (c) vertical stress distribution. State C: (d) vertical stress distribution

edge and the corresponding horizontal force F. The *low wall* exhibits a limit strength followed by a post-peak behaviour, with a significant stiffness degradation and increase of the dissipation. On the contrary, the cyclic response of the *high wall* points out the presence of an overturning mechanism, with low degradation and dissipation.

The theoretical simulations are shown in Figures 11(c) and 11(d), from which it can be seen that the proposed composite model is able to take in both the stiffness and the collapse load of the two walls and to discriminate between the different collapse mechanisms. The two simulations are obviously obtained by the same model parameters, which are shown in Table IV. The compressive strength of the masonry $\sigma_{Mr} = 5$ MPa and the following softening branch have been synthesized in the post-elastic model of the brick elements.

With reference to the *low wall*, the mortar joint damage at state A (corresponding to the peak load), is shown in Figures 12(a) and 12(b) concerning the sliding and opening damage, respectively. It emerges that opening mechanisms are attained in the corners of the wall while sliding is distributed in a central vertical domain. Moreover, it is worth noting that at this state no head mortar joint has undergone rupture.

A detailed description of the train of mechanisms which became active in the post-peak phase is supplied by the distribution of the broken mortar joints undergoing opening (Figures 13(a) and 13(b)). The significant loss of strength after the peak load (state B) is due to the activation of openings of the head mortar joint in the

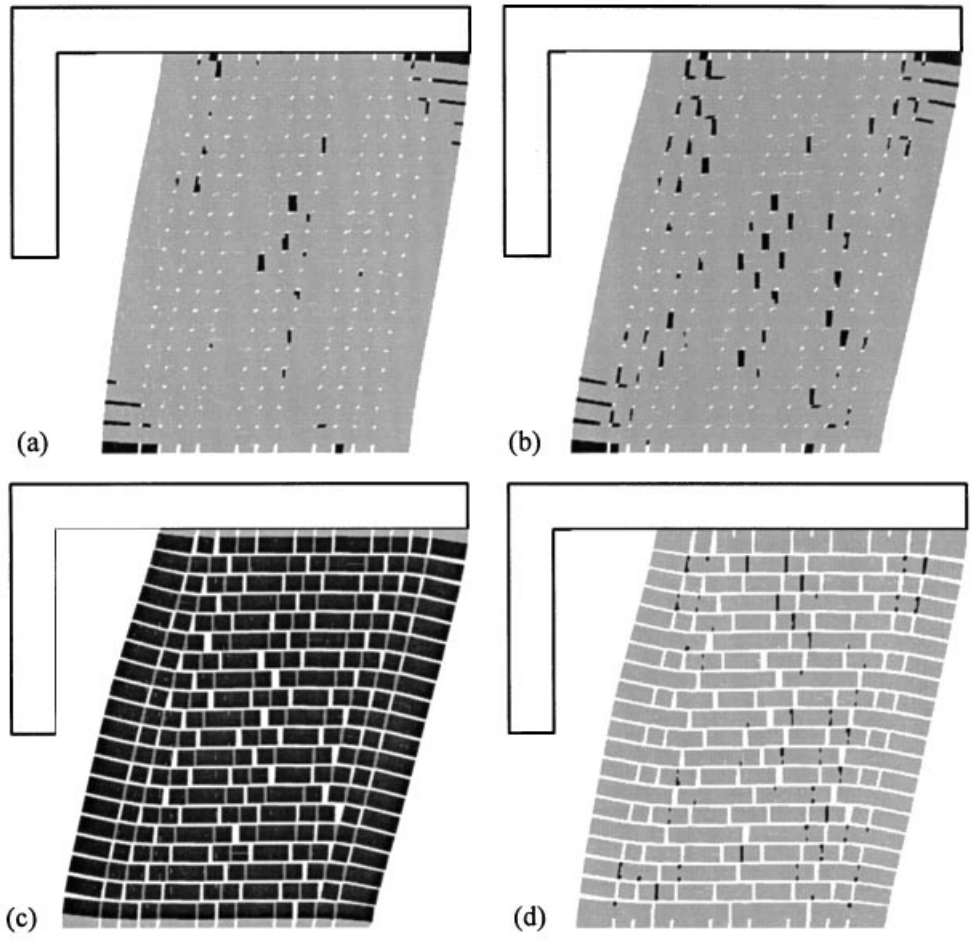

Figure 13. *Low wall*. Opening rupture of mortar joints: (a) state B, (b) state C. (c) Wall configuration at the state C. (d) Rupture in the bricks at the state C

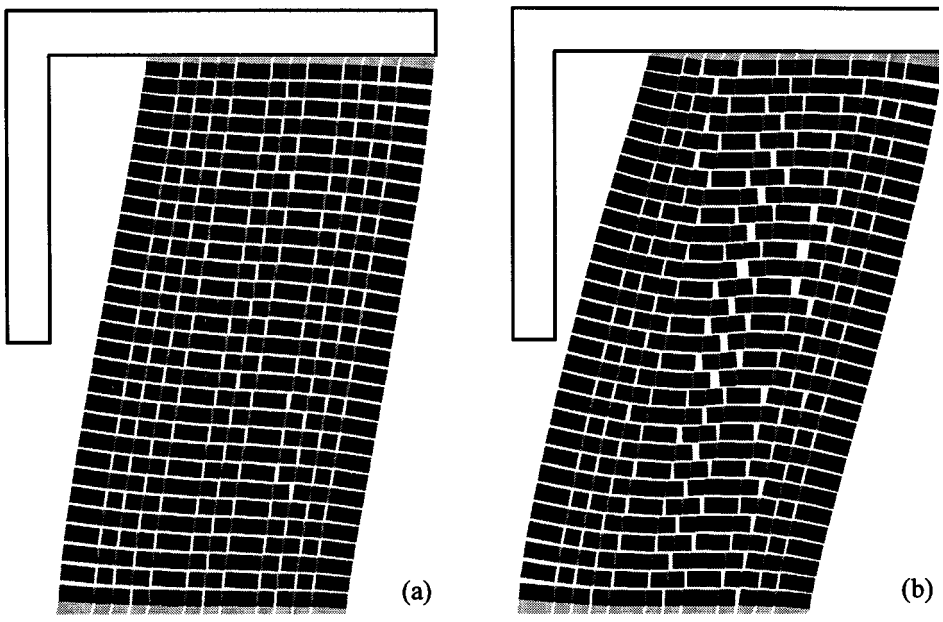

Figure 14. Configuration of the *high wall*: (a) $v = 7{\cdot}5$ mm; (b) $v = 10$ mm

middle of the wall together with sliding mechanisms in the bed mortar joints (Figure 13(a)). In the cycles of the widest amplitude the wall exhibits also the rupture due to the opening of the head mortar joints in the lateral portions (Figure (13b)); these last mechanisms are activated by the flexural rupture of some bricks, as can be seen in Figure 13(d), where the brick interfaces which fail are represented in black.

The evolution of the stress distribution from state A to state C is shown by Figures 12(c) and 12(d) where it emerges as a transition from an equilibrium state characterized by a compressed diagonal band to another one in which two compressed inclined bands appear, due to rupture of bed and head mortar joints in the central domain.

Finally, the considerable hysteretic dissipation is probably due to an underestimation of the brittleness of the brick interfaces. However, it is worth noting that the above-described damage evolution agrees with that observed in the wall during the experimental test.[2]

The different behaviour of the *high wall* may be evinced by Figure 14(a), which represents the wall configuration in the point A (Figure 11(d)) and shows significant openings of the bed joints in the corners due to an overturning mechanism. After this point the theoretical response swerves from the experimental one, showing a loss of strength and an increase of the hysteretic dissipation due to the activation of sliding mechanisms in the middle of the wall along a vertical band (point B in Figure 11(d)); this fact may be observed in Figure 14(b), which shows that the head mortar joints in the middle of the wall get opened while no brick fails for bending around the corners. However, it is worth noting that in the experimental test this mechanism has been observed in the cycles of amplitude 12·5 mm, as a proof that the transition between the two collapse mechanisms is characteristic of this wall as well.

5. CONCLUSIONS

In this paper a damage model for mortar joints is proposed, which considers both the mortar damage and the decohesion in the mortar–brick interface. The inelastic strain components, i.e. the extension and sliding of the mortar joint, are assumed linearly dependent on the mean stress and a damage variable, whose evolution is

ruled in accordance with a damage mechanics approach. Moreover, the sliding is limited by the presence of the friction in the brick–mortar interface, that produces the hysteretic response of the joint under cyclic shearing strains.

The model capabilities have been verified by the simulation of shear bond tests, carried out both by triplets and by a direct shear apparatus. It is worth noting that all the model parameters may be obtained by the results of experimental tests on brick–mortar assemblies.

This model has been applied in the analysis of brick masonry walls under vertical constant loads and horizontal cyclic forces by means of a composite finite element model made up of inelastic brick units and mortar joints. This approach gives a detailed description of the different mechanisms of inelasticity which are characteristic of brick masonry walls: the opening and sliding of the bed and head mortar joints, the tensile and shearing rupture of bricks and the compressive failure of masonry.

Also, in this case the capability of the above-mentioned scheme of analysis has been verified by simulating some experimental results carried out on two walls of different shape but made up with the same masonry pattern and units.

As this model seems to be too burdensome in analysing full-scale masonry walls with openings, a continuum model will be proposed in the companion paper.[1] However, the composite model may form a reliable support in the definition of the validity limits of the continuum model, in which some of the above-mentioned inelastic mechanisms will be neglected.

ACKNOWLEDGEMENTS

The present research was carried out with the financial support of the Italian National Research Council C.N.R.-G.N.D.T.

REFERENCES

1. G. Gambarotta and S. Lagomarsino, 'Damage models for the seismic response of brick masonry shear walls. Part II: The continuum model and its application', *Earthquake eng. struct. dyn.* **26**, 441–462 (1997).
2. A. Anthoine, G. Magonette and G. Magenes, 'Shear-compression testing and analysis of brick masonry walls', in G. Duma (ed.), *Proc. 10th European conf. on earthquake eng.*, Vol. 3, *Balkema*, *Rotterdam*, 1995, pp. 1657–1662.
3. D. Benedetti and G. M. Benzoni, 'A numerical model for seismic analysis of masonry buildings: Experimental Correlations', *Earthquake eng. struct. dyn.* **12**, 817–831 (1984).
4. M. Tomazevic, 'Dynamic modelling of masonry buildings: Storey mechanism model as a simple alternative', *Earthquake eng. struct. dyn.* **15**, 731–749 (1987).
5. G. Del Piero, 'Constitutive equation and compatibility of the external loads for linearly elastic masonry-like materials', *Meccanica* **24**, 150–162 (1989).
6. H. R. Lofti and P. B. Shing, 'An appraisal of smeared crack models for masonry shear wall analysis', *Comput. struct.* **41**, 413–425 (1991).
7. J. G. Rots, 'Numerical simulation of cracking in structural masonry', *Heron* **36**, 49–63 (1991).
8. C. Ignatakis, E. Stavrakakis and G. Penelis, 'Analytical model for masonry using the finite element method', *Structural repair and maintenance of historical buildings*, Computational Mechanics Publications, 1989, pp. 511–523.
9. A. W. Page, 'Finite element model for masonry', *J. struct. eng. div. ASCE* **104**, 1267–1285 (1978).
10. H. R. Lofti and P. Benson Shing, 'Interface model applied to fracture of masonry structures', *J. struct. eng. div. ASCE* **120** (1), 63–80 (1994).
11. P. B. Lourenço, J. G. Rots and J. Blaauwendraad, 'Implementation of an interface cap model for the analysis of masonry structures', in *Proc. int. conf. computational modeling of concrete structures*, pp. 123–134, Innsbruck, 1994.
12. L. Gambarotta and S. Lagomarsino. 'Damage in brick masonry shear walls', in Z. P. Bazant, Z. Bittnar, M. Jirásek and J. Mazars (eds), *Fracture and Damage in Quasibrittle Structures*: *Experiment*, *Modeling and Computer Analysis*, Prague, 1994, pp. 463–472.
13. S. Pietruszczak, 'On mechanics of jointed media: Masonry and related problems', in G. Beer, J. R. Booker and J. P. Carter (eds) *Computer methods and Advances in Geomechanics*, Vol. 2, Balkema, Rotterdam, Brookfield, 1991, pp. 407–415.
14. S. Pietruszczak and X. Niu, 'A methematical description of macroscopic behaviour of brick masonry', *Int. j. solids Struct.* **29**, 531–546 (1992).
15. G. Alpa and I. Monetto, 'Microstructural model for dry blok masonry walls with in-plane loading', *J. mech. phys. solids* **42**, 1159–1175 (1994).
16. A. Anthoine, 'Derivation of the in-plane elastic characteristics of masonry through homogenization theory', *Int. j. solids struct.* **32**, 137–163 (1995).

17. G. N. Pande, J. X. Liang and J. Middleton, 'Equivalent elastic moduli for brick masonry', *Comput. geotech.* **8**, 243–265 (1989).
18. G. Maier, A. Nappi and E. Papa, 'Damage models for masonry as a composite materials: a numerical and experimental analysis', in C. S. Desai, E. Krempl, G. Frantiziskonis and H. Saadatmanesh (eds), *Constitutive Laws for Engineering Materials* ASME, New York, 1991, pp. 427–432.
19. R. H. Aktinson, P. B. Amadei, S. Saeb and S. Sture, 'Response of masonry bed joints in direct shear', *J. struct. eng. div. ASCE* **115**, 2276–2296 (1989).
20. R. van der Pluijm, 'Shear behaviour of bed joints', in *Proc. 6th North American masonry conf.*, Vol. 1, Philadelphia, 1993, pp. 125–136.
21. L. Binda, G. Mirabella, C. Tiraboschi and S. Abbaneo, 'Measuring masonry material properties', in D.P. Abrams and G.M. Calvi (eds), *Proc. U.S.-Italy workshop on guidelines for seismic evaluation and rehabilitation of unreinforced masonry buildings*, State Univ. of New York at Buffalo, NCEER-94-0021, 6-3/24, Pavia, 1994.
22. S. Nemat-Nasser and M. Hori, *Micromechanics: Overall Properties of Heterogeneous Materials*, Elsevier, Amsterdam, 1993.
23. L. Gambarotta and S. Lagomarsino, 'A microcrack damage model for brittle materials', *Int. j. solids struct.* **30**, 177–198 (1993).
24. M. Plesha, R. Ballarini and A. Parulekar, 'Constitutive model and finite element procedure for dilatant contact problems', *J. eng. mech. div. ASCE* **115**, 2649–2668 (1989).
25. M. P. Divakar and A. Fafitis, 'Micromechanics-based constitutive model for interface shear', *J. eng. mech. div. ASCE* **118**, 1317–1337 (1992).
26. O. Zienkiewicz and R. L. Taylor, *The Finite Element Method*, Vol. 2, McGraw-Hill, London, 1991.
27. J. C. Simo, J. G. Kennedy and S. Govindjee, 'Non-smooth multisurface plasticity and viscoplasticity. Loading and unloading conditions and numerical algorithms', *Int. j. numer. methods eng.* **26**, 2161–2185 (1988).
28. J. C. J. Schellekens and R. de Borst, 'On the numerical integration of interface elements', *Int. j. numer. methods eng.* **36**, 43–66 (1993).

